Available online at www.sciencedirect.com
SciVerse ScienceDirect
Ceramics International 38 (2012) 5089–5093
CERAMICS INTERNATIONAL
www.elsevier.com/locate/ceramint

# Synthesis, characterization and electrochemical performance of $Sn_3F_3PO_4$ anode material for lithium-ion batteries

Sofiane Bouazza *, Ali Saberi, Monika Willert-Porada

*Chair of Materials Processing, Faculty of Engineering Science, University of Bayreuth, 95440 Bayreuth, Germany*

Received 6 February 2012; received in revised form 2 March 2012; accepted 3 March 2012
Available online 12 March 2012

**Abstract**

Tin fluorophosphate ($Sn_3F_3PO_4$) powder was synthesized via a microemulsion route. Physical properties of the synthesized material were investigated by means of X-ray powder diffractometry (XRD) and field emission scanning electron microscopy (FE-SEM). The investigation showed that the synthesized powder was crystalline $Sn_3F_3PO_4$ with needle-like morphology with a thickness of 300–500 nm and length of 5–10 μm. The electrochemical performance of the synthesized powder as a negative electrode for Li-ion batteries was studied. The results showed that the synthesized $Sm_3F_3PO_4$ possessed an initial discharge capacity of 1370 mAh $g^{-1}$ and charge capacity of 968 mAh $g^{-1}$ in a potential range of 0.005–3 V. In addition, the material showed capacity retention of 70.8% after 30 cycles at a constant current density of 100 mA $g^{-1}$.
© 2012 Elsevier Ltd and Techna Group S.r.l. All rights reserved.

*Keywords:* A. Powders: chemical preparation; C. Electrical properties; E. Electrodes; E. Batteries; $Sn_3F_3PO_4$

## 1. Introduction

The energy density and performance of lithium-ion batteries depend highly on the physical and chemical properties of the cathode and anode materials. Although commercially used graphite anodes have good electrochemical properties, their low theoretical capacity (372 mAh $g^{-1}$) is insufficient to satisfy the market requirements. To achieve batteries with higher energy density, silicon (4200 mAh $g^{-1}$) [1] and tin (992 mAh $g^{-1}$) [2], which alloy reversibly with lithium, have been considered as a replacement for graphite [3–5]. However, the large volume change upon lithiation is the main drawback of these metal elements [6,7]. Several approaches have been proposed to deal with the problem of volume expansion. One of the most effective ways is to fabricate an electrode based on nanostructures such as nanoparticles, nanowires, nanotubes or porous nanostructures [8–10]. Owing to its small size, the nanosized Sn-based anode can reduce the volume change and restrain stress; moreover, the high surface/volume ratio increases the electrode–electrolyte interface and promotes faster diffusion of $Li^+$ ions into the material so that a higher charging rate is possible [11,12].

Another approach is to integrate host (Si or Sn) with an intermetallic phase and/or to make composite based on active- and less active materials (alloying the active metal with less active or even electrochemically inactive matrix) to limit the overall volume expansion of the reactant and improve cyclability of the electrode [2,6,13,14]. As a step forward, development of inactive matrix during the first lithiation has been suggested. For example in the case of tin based electrodes, tin oxide, phosphate, and fluoride were applied [15–19]. The authors have synthesized and characterized $SnF_2$ as a negative electrode for lithium-ion batteries [16]. The investigations on tin oxide showed an irreversible conversion of $SnO_2$ to tin according to (R.1) in the first cycle. Subsequently, the in situ formed metallic tin phase can store and release Li ions according to the Li–Sn alloying and de-alloying reactions (R.2):

$$SnO_2 + 4Li^+ + 4e^- \rightarrow Sn + 2Li_2O \quad (R.1)$$

$$Sn + xLi^+ + xe^- \leftrightarrow Li_xSn \quad (0 \leq x \leq 4.4) \quad (R.2)$$

The promising results obtained by applying tin fluoride and tin phosphates instead of metallic tin as negative electrode in lithium ion batteries have drawn the authors' attention to

* Corresponding author. Tel.: +49 0921 557208; fax: +49 0921 557205.
*E-mail address:* bouazza_sofiane@yahoo.fr (S. Bouazza).

0272-8842/$36.00 © 2012 Elsevier Ltd and Techna Group S.r.l. All rights reserved.
doi:10.1016/j.ceramint.2012.03.011

synthesize and characterize a tin-containing phase in the ternary system of Sn(II)-F-$PO_4$ for the same application.

Metal fluorophosphates like titanium (IV) fluorophosphates [20], zirconium phosphate fluorides [21], gallium phosphate fluorides [22] and tin fluorophosphate [23] have been mainly synthesized using organic template molecules under hydrothermal conditions. To the best of authors' knowledge, the more stable phase in this ternary system is $Sn_3F_3PO_4$ with a rhombohedral structure. The most of studies on $Sn_3F_3PO_4$ were mainly done for dentistry in 70s, where the rate of $Sn_3F_3PO_4$ formation subsequent to in vitro $SnF_2$ interaction with human dental mineral (R.3) was the point of interest. The formed $Sn_3F_3PO_4$ showed more resistance to decay than the dental enamel [24,25].

$$18SnF_2 + Ca_{10}(PO_4)_6(OH)_2 \rightarrow 6Sn_3F_3PO_4 + 9CaF_2 + Ca(OH)_2 \quad \text{(R.3)}$$

Salami et al. [23] were the only group which have synthesized $Sn_3F_3PO_4$ powder for another application. They have synthesized $Sn_3F_3PO_4$ with needle-like morphology using hydrothermal reaction between hydrofluoric acid, tin (II) fluoride, boric acid, and a phosphate source such as hexafluorophosphoric acid ($HPF_6$) or tetra-*n*-butylammonium hexafluorophosphate ($(C_4H_9)_4NPF_6$) in a mixture of distilled water and pyridine in an autoclave at 150 °C for 5 days. They claimed the synthesized powder has potential to be used as molecular sieve because it possesses an open framework.

The aim of this study was the synthesis of $Sn_3F_3PO_4$ fine powder via the reaction of tin (II) fluoride and phosphoric acid in inverse micelles (water-in-oil inverse microemulsion) at low temperatures and subsequently evaluating its electrochemical performance as anode material for lithium-ion batteries using galvanostatic cycling and cyclic voltammetry (CV).

## 2. Experimental procedure

### 2.1. Synthesis of $Sn_3F_3PO_4$ powder

All reagents were commercially available products and used without further purification. Tin fluoride (99%, $SnF_2$), Igepal CO-520 (polyoxyethylene (5) nonylphenylether, $M_n \sim 441$), cyclohexane (≥99%, $C_6H_{12}$), 1-hexanol (≥99%, $C_6H_{14}O$), and phosphoric acid (85 wt.% in $H_2O$, $H_3PO_4$) were purchased from Sigma–Aldrich Chemical Co. In a typical synthesis, 34 mmol of Igepal CO-520 and 48 mmol of 1-hexanol were added into a reaction vessel, a 250 ml PTFE round bottom flask, containing 1.8 mol of cyclohexane. The mixture was stirred at 40 °C for 30 min. Igepal CO-520 and 1-hexanol were respectively chosen as the surfactant and co-surfactant. The basic concept of the microemulsion process is dispersion of the aqueous phase as tiny drops into the oil phase using a surfactant and co-surfactant in order to confine the growth of particles precipitating within [26,27]. Subsequently, 3.94 mmol of phosphoric acid was drop-wise introduced into the respective solution. After 5 min mixing, 11.8 mmol of $SnF_2$ which was separately dissolved in 0.25 mol of distilled water was added to the previous solution while stirring. The resulting microemulsion solution was stirred vigorously at 40 °C under reflux for 30 min on a magnetic hot plate stirrer. The resulting suspension was allowed to cool down to room temperature and the precipitated particles were collected by centrifugation and washed several times with plenty of methanol to remove the non-polar solvent and surfactants. Afterward the obtained powder was dried at 60 °C for 6 h.

### 2.2. Characterization

The synthesized powder was characterized with a Philips (PW-3040) X-ray diffractometer (XRD) with Cu-$K_\alpha$ radiation. The JCPDF card No. 01-076-2280 was used for the identification of $Sn_3F_3PO_4$. The apparent crystallite size of the synthesized tin fluorophosphate was determined using the Scherrer equation (Eq. (1)):

$$\beta(2\theta) = \frac{k \cdot \lambda}{L \cdot \cos\theta_0} \quad (1)$$

where $\lambda$ is the wavelength (=0.15406 nm), $\theta_0$ the Bragg angle, $k$ a constant (=0.9), and $L$ is the apparent crystallite size. The half-width of the diffraction line $\beta(2\theta)$ (in rad) was taken as the experimental half-width ($\beta_{exp}$) and corrected for experimental broading ($\beta_{instr}$) according to Eq. (2) [28]:

$$\beta(2\theta) = (\beta_{exp}^2 - \beta_{instr}^2)^{1/2} \quad (2)$$

$\beta_{instr}$ was measured experimentally with a silicon sample as standard. For this purpose three diffraction peaks (1 1 0), (1 0 1), and (1 3 1), which have the advantage of being well separated from other peaks, were chosen for the calculation.

A field emission scanning electron microscope (LEO® 1530, FE-SEM) was utilized to determine the particle morphology and to assess the size of synthesized particles. To prepare the sample for microscopic investigation, the powders were dispersed in ethanol by ultrasonication for 10 min, and the resultant suspension was spread on the surface of an aluminum plate and subsequently coated with a 2 nm thick platinum layer to prevent electron charge on the surface of particles during electron microscopy.

The electrochemical characterization of synthesized $Sn_3F_3PO_4$ was measured using two electrodes in a Swagelok-type cell assembled under argon atmosphere. The working electrode consisted of $Sn_3F_3PO_4$ (60 wt.%), carbon black (28 wt.%) and polyacrylonitrile (PAN) (12%) dissolved in dimethyl sulfoxide (DMSO). The slurry was cast on a copper foil with a doctor blade apparatus, the coated copper foil was dried at 80 °C for 6 h to remove the residual solvent, and subsequently was heat treated at 300 °C for 3 h. Glass-fiber filter paper (GF/D) from Whatman® was used as separator. Lithium foil was used as the counter and the reference electrodes. A solution of 1 M $LiPF_6$ in a 1:1 volume ratio mixture of ethylene carbonate (EC) and dimethyl carbonate (DMC) was used as electrolyte. Cyclic voltammetry and charge/discharge cycling were carried out between 0.005 and 3 V using a Basytec cell test system.

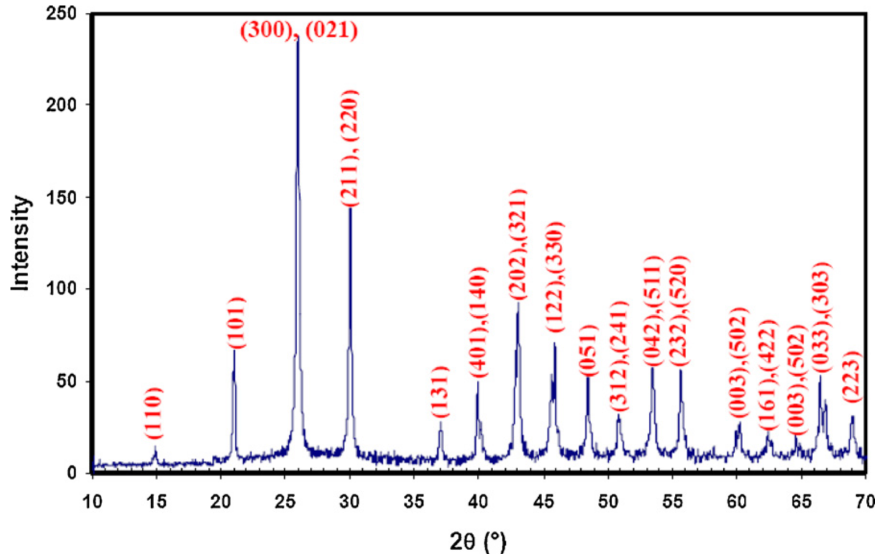


Fig. 1. XRD pattern of the synthesized tin fluorophosphate powder.

## 3. Results and discussion

Fig. 1 illustrates X-ray diffraction pattern of the synthesized powder. The synthesized powder was a poly crystalline $Sn_3F_3PO_4$ formed via (R.4) in the reaction vessel. The pattern corresponds to the reported XRD pattern by Jordan et al. [25]. According to the Scherrer equation, the crystallite size of synthesized $Sn_3F_3PO_4$ powder was in the range of 50–55 nm.

$$3SnF_2 + H_3PO_4 \rightarrow Sn_3F_3PO_4 + 3HF \qquad (R.4)$$

The FE-SEM micrograph indicates that the synthesized powder had a needle-like morphology with a thickness of 300–500 nm and length of 5–10 μm (Fig. 2). The powder had the same morphology as $Sn_3F_3PO_4$ powder synthesized by Salami et al. [23], needle like particles with a thickness of few microns and length of 300–500 μm. Due to the considerably lower reaction temperature (40 °C) and dwell time (30 min) applied in the current study in comparison with those of applied by Salami et al. (150 °C, 120 h), the needles were at least 30 times shorter.

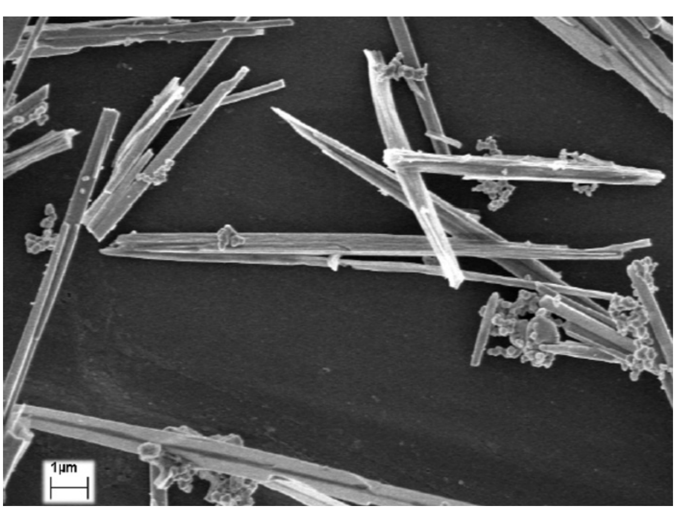


Fig. 2. FE-SEM micrograph of synthesized $Sn_3F_3PO_4$.

The $Li^+$ insertion/extraction reactions of the $Sn_3F_3PO_4$ electrode were studied by cyclic voltammetry (Fig. 3). A substantial difference between the first and all subsequent cycles was observed. Two reduction peaks at 1.64 V and 1.46 V during the first cycle might correspond to the decomposition of $Sn_3F_3PO_4$ into Sn and formation of $Li_3PO_4$ and LiF according to reaction (R.5). When the electrode was completely activated, the mentioned peaks were not observed any more in subsequent cycles but instead a low intensity redox pair was identified at 1.88 and 2.10 V. It means that (R.5) is partially reversible during the second and third cycles.

$$Sn_3F_3PO_4 + 6Li^+ + 6e^- \rightarrow 3Sn + 3LiF + Li_3PO_4 \qquad (R.5)$$

The disappearance of third cathodic peak at 0.71 V on the second cathodic sweep could be attributed to solid-electrolyte interface (SEI) formation [29]. The other redox pairs during discharge (at 0.5, 015 V) and charge cycles (at 0.58, 1.06 V) were related to the reversible $Li_xSn$ formation [30] given by reaction (R.6).

$$Sn + xLi^+ + xe^- \leftrightarrow Li_xSn \quad (0 \leq x \leq 4.4) \qquad (R.6)$$

Therefore $Li^+$ storage capacity can be mainly attributed to alloying/de-alloying of metallic tin with partial contribution of redox system (R.6) at high potentials.

The electrochemical performance of $Sn_3F_3PO_4$ as an anode material for lithium ion-batteries was tested in the potential range 0.05–3 V (versus $Li/Li^+$). The initial open circuit voltage (OCV) of the $Sn_3F_3PO_4$/Li half cell was 2.8 V. Fig. 4a shows the typical galvanostatic cycling profiles of the tin fluorophosphate electrode at a specific current of 100 mA $g^{-1}$. The potential dropped rapidly to 1.7 V and demonstrated a discharge plateau between 1.65 and 1.4 V. As reported for tin-based

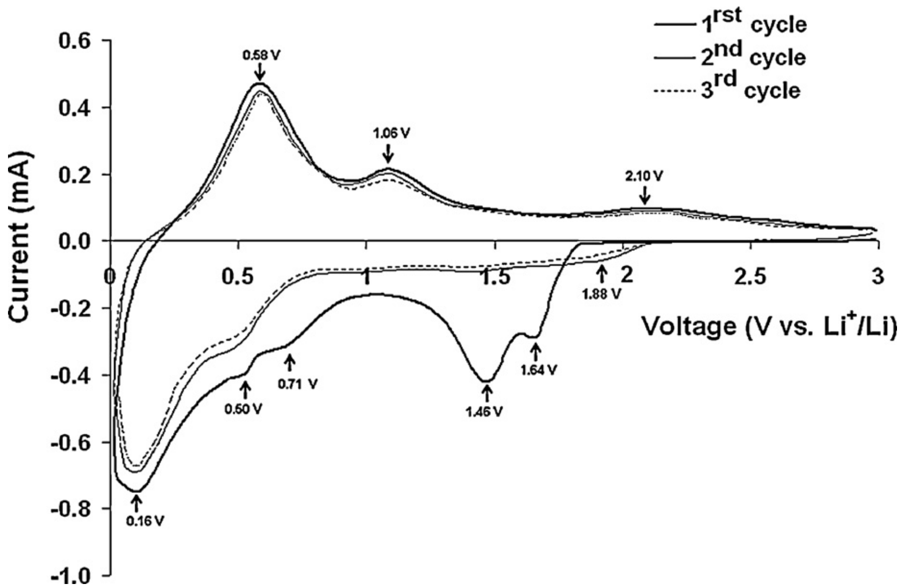


Fig. 3. Cyclic voltammograms of tin fluorophosphate electrode at a scan rate of 0.05 mV $s^{-1}$.

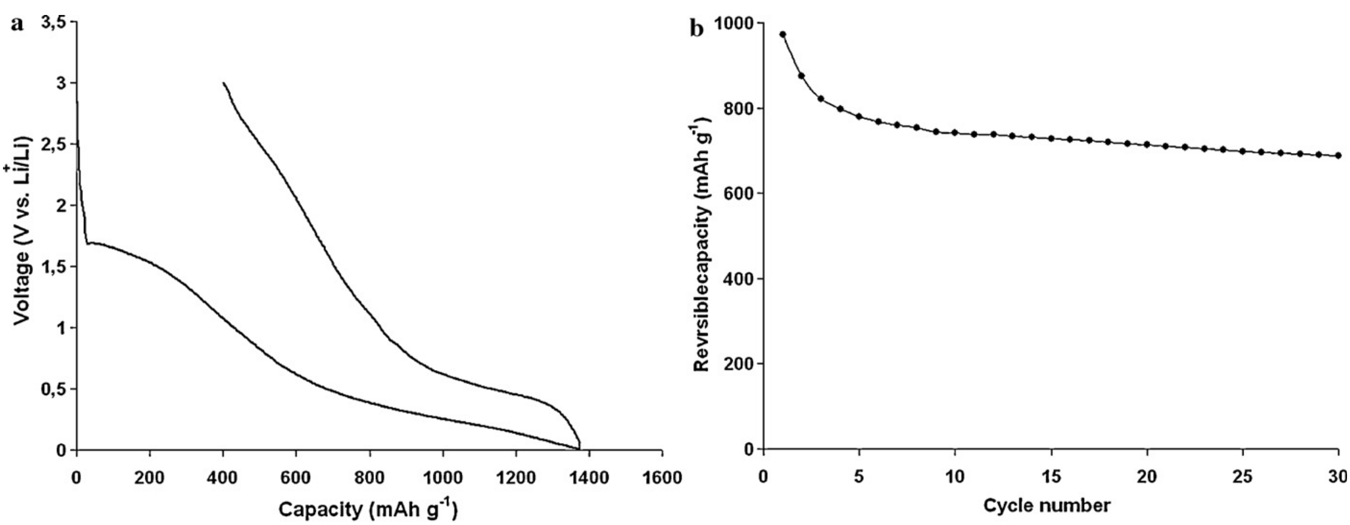


Fig. 4. First charge/discharge profile (a) and cyclic performance of $Sn_3F_3PO_4$ anode at a current density of 100 mA $g^{-1}$ (b).

anodes [18] the first plateau at high voltages was assigned to the decomposition of the tin-based anode into metallic tin (R.5). During the following reaction stage, the potential drops slowly from 0.5 to 0.05 V, this corresponded to the alloying/dealloying of Li and Sn. As it can be seen from the charge/discharge profile, the $Sn_3F_3PO_4$ electrode delivered an initial discharge capacity of 1370 mAh $g^{-1}$ and charge capacity of 972 mAh $g^{-1}$, showing a superior lithium storage capacity. Such a large irreversible capacity loss could be assigned to the consumption of $Li^+$ ions during the reduction of $Sn_3F_3PO_4$ to metallic Sn (R.5) and also to the formation of a solid-electrolyte interface (SEI) during the first charge/discharge process. After 30 cycles (Fig. 4b), the material ($Sn_3F_3PO_4$) showed a stable reversible capacity of 688 mAh $g^{-1}$which corresponds to 70.8% retention of its initial capacity.

## 4. Conclusions

In summary, tin fluorophosphate ($Sn_3F_3PO_4$) was successfully synthesized via a microemulsion route at 40 °C. The synthesized powder had a needle-like morphology with a thickness of 300–500 nm and length of 5–10 μm. Electrochemical measurements indicated that the anode material based on crystalline $Sn_3F_3PO_4$ displayed a highly reversible capacity with the initial discharge and charge capacity of 1370 and 972 mAh $g^{-1}$, respectively. The cyclic voltammetry study revealed that the electrochemical process in tin fluorophosphates is similar to Sn-oxide and Sn-phosphate systems. Furthermore, high capacity of 688 mAh $g^{-1}$ after 30 cycles at a current density of 100 mAh $g^{-1}$ made this material a good candidate as a negative electrode for lithium-ion batteries.

## Acknowledgment

The authors would like to thank Dr.-Ing. Zahra Negahdari for her great help in scanning electron microscopy.

## References

[1] M.N. Obrovac, L. Christensen, Structural changes in silicon anodes during lithium insertion/extraction, Electrochem. Solid-State Lett. 7 (2004) A93–A96.

[2] M. Wachtler, J.O. Besenhard, M. Winter, Tin and tin-based intermetallics as new anode materials for lithium-ion cells, J. Power Sources 94 (2001) 189–193.

[3] H. Wolf, Z. Pajkic, T. Gerdes, M. Willert-Porada, Carbon–fiber–silicon-nanocomposites for lithium-ion battery anodes by microwave plasma chemical vapor deposition, J. Power Sources 190 (2009) 157–161.

[4] W. Choi, J. Yong Lee, B.H. Jung, H.S. Lim, Microstructure and electrochemical properties of a nanometer-scale tin anode for lithium secondary batteries, J. Power Sources 136 (1999) 154–159.

[5] Y. Idota, T. Kubota, A. Matsufuji, Y. Maekawa, T. Miyasaka, Tin-based amorphous oxide: a high-capacity lithium-ion-storage material, Science 276 (1997) 1395–1397.

[6] M. Winter, J.O. Besenhard, Electrochemical lithiation of tin and tin-based intermetallics and composites, Electrochim. Acta 45 (1999) 31–50.

[7] R. Nesper, Structure and chemical bonding in Zintl-phases containing lithium, Prog. Solid State Chem. 20 (1990) 1–45.

[8] J. Yao, X. Shen, B. Wang, H. Liu, G. Wang, In situ chemical synthesis of $SnO_2$–graphene nanocomposite as anode materials for lithium-ion batteries, Electrochem. Commun. 11 (2009) 1849–1852.

[9] N.H. Zhao, L.C. Yang, P. Zhang, G.J. Wang, B. Wang, B.D. Yao, Y.P. Wu, Polycrystalline $SnO_2$ nanowires coated with amorphous carbon nanotube as anode material for lithium ion batteries, Mater. Lett. 64 (2010) 972–975.

[10] Z. Wen, Q. Wang, Q. Zhang, J. Li, In situ growth of mesoporous $SnO_2$ on multiwalled carbon nanotubes: a novel composite with porous-tube structure as anode for lithium batteries, Adv. Funct. Mater. 17 (2007) 2772–2778.

[11] J.O. Besenhard, J. Yang, M. Winter, Will advanced lithium-alloy anodes have a chance in lithium-ion batteries? J. Power Sources 68 (1997) 87–90.

[12] N. Pereira, L.C. Klein, G.G. Amatucci, Particle size and multiphase effects on cycling stability using tin-based materials, Solid State Ionics 167 (2004) 29–40.

[13] R. Ewa, J. Yin, K. Akiko, W. Masahi, S. Tetsuo, Comparative studies of mechanical and electrochemical lithiation of intermetallic nanocomposite alloys for anode materials in Li-ion batteries, Solid State Ionics 176 (2005) 2749–2757.

[14] B. Guo, J. Shu, K. Tang, Y. Bai, Z. Wang, L. Chen, Nano-Sn/hard carbon composite anode material with high-initial coulombic efficiency, J. Power Sources 177 (2008) 205–210.

[15] I.A. Courtney, J.R. Dahn, Key factors controlling the reversibility of the reaction of lithium with $SnO_2$ and $Sn_2BPO_6$ glass, J. Electrochem. Soc. 144 (1997) 2943–2948.

[16] S. Bouazza, A. Saberi, M. Willert-Porada, Preparation and electrochemical properties of nano-sized $SnF_2$ as negative electrode for lithium-ion batteries, Mater. Lett. 65 (2011) 1334–1336.

[17] S. Attidekou, O.A. Connor, P. Wormald, D.P. Tinstall, S.M. Francis, J.T.S. Irvine, Solid state NMR studies of phosphate/tin matrix formed on electrochemical insertion into $SnP_2O_7$, Solid State Ionics 175 (2004) 185–190.

[18] L. Li, X. Yin, S. Liu, Y. Wang, L. Chen, T. Wang, Electrospun porous $SnO_2$ nanotubes as high capacity anode materials for lithium ion batteries, Electrochem. Commun. 12 (2010) 1383–1386.

[19] M.S. Park, Y.M. Kang, G.-X. Wang, S.-X. Dou, H.-K. Liu, The effect of morphological modification on the electrochemical properties of $SnO_2$ nanomaterials, Adv. Funct. Mater. 18 (2008) 455–461.

[20] M. Wloka, S. Trozanov, E. Kemnitz, Structural study of the dehydration of templated zirconium phosphate fluorides, Solid State Sci. 4 (2002) 1377–1383.

[21] C. Serre, M. Hervieu, C. Magnier, F. Taulelle, G. Ferey, Synthesis and characterization of mesostructured titanium(IV) fluorophosphates with a semicrystalline inorganic framework, Chem. Mater. 14 (2002) 180–188.

[22] R.I. Walton, F. Millange, A. Le Bail, T. Loiseau, C. Serre, D. O'Hare, G. Ferey, The room-temperature crystallisation of a one-dimensional gallium fluorophosphate, $Ga(HPO_4)_2F{\cdot}H_3N(CH_2)$ $3NH_3{\cdot}2H_2O$, a precursor to three-dimensional microporous gallium fluorophosphates, Chem. Commun. 3 (2000) 203–204.

[23] T.O. Salami, P.Y. Zavalij, S.R.J. Oliver, Synthesis and crystal structure of two tin fluoride materials: $NaSnF_3$ (BING-12) and $Sn_3F_3PO_4$, J. Solid State Chem. 177 (2004) 800–805.

[24] J.C. Muhler, W.H. Nebergall, H.G. Day, Studies on stannous fluoride and other fluorides in relation to the solubility of enamel in acid and the prevention of experimental dental caries, J. Dent. Res. 33 (1954) 33–49.

[25] T.H. Jordan, S.H.Y. Wei, S.H. Bromberger, J.C. King, $Sn_3F_3PO_4$: the product of the reaction between stannous fluoride and hydroxyapatite, Arch. Oral Biol. 16 (1971) 241–246.

[26] M. Ganguli, D. Ganguli, Inorganic Particle Synthesis via Macro- and Microemulsions a Micrometer to Nanometer Landscape, Kluwer Acad., Plenum Publ., 2003.

[27] A. Saberi, Z. Negahdari, S. Bouazza, M. Willert-Porada, Synthesis and characterization of crystalline nanosized $MgF_2$ powder via microemulsion route, J. Fluorine Chem. 131 (2010) 1353–1355.

[28] P. Klug, L.E. Alexander, X-ray Diffraction Procedure for Polycrystalline and Amorphous Materials, Wiley, New York, 1974.

[29] H. Bryngelsson, J. Eskhult, L. Nyholm, M. Herranen, O. Alm, K. Edstrom, Electrodeposited Sb and $Sb/Sb_2O_3$ nanoparticle coatings as anode materials for Li-ion batteries, Chem. Mater. 19 (2007) 1170–1180.

[30] J.S Chen, Y.L. Cheah, Y.T. Chen, N. Jayaprakash, S. Madhavi, Y.H. Yang, X.W. Lou, $SnO_2$ nanoparticles with controlled carbon nanocoating as high-capacity anode materials for lithium-ion batteries, J. Phys. Chem. C 113 (2009) 20504–20508.